引用格式：MA Fengxiang, ZHAO Yue, WANG Nan, et al. High-sensitivity Detection Technology of SF_6 Decomposition Product H_2S Based on Multi-pass Photoacoustic Cell[J]. Acta Photonica Sinica, 2023, 52(3):0352121
马凤翔,赵跃,王楠,等.基于多通光声池的SF_6分解产物H_2S的高灵敏度检测技术[J].光子学报,2023,52(3):0352121

基于多通光声池的SF_6分解产物H_2S的高灵敏度检测技术

马凤翔[1],赵跃[1],王楠[2],赵新瑜[2],郭珉[2],李辰溪[2],朱太云[1],杭忱[1],陈珂[2]
(1 国网安徽省电力有限公司 电力科学研究院,合肥 230601)
(2 大连理工大学 光电工程与仪器科学学院,大连 116024)

摘 要:针对H_2S气体在近红外波段的吸收系数低导致检测灵敏度难以提高的难题,提出了基于共振式多通光声池的SF_6分解产物H_2S气体检测技术。对赫里奥特型多通光声池进行优化设计,激光光束反射次数达到20次。近红外激光经功率放大后入射到多通光声池,通过多次光学反射大幅度提升了光声信号的激发效率,结合声学共振放大技术、光纤放大技术和波长调制-二次谐波检测技术,搭建了一套光声光谱气体检测系统,实现了SF_6背景下微量H_2S气体的高灵敏度检测。实验结果表明,归一化噪声等效吸收系数为2.23×10^{-9} $cm^{-1}\cdot W\cdot Hz^{-1/2}$,在平均时间为100 s时,该检测系统对$H_2S$气体的检测极限达到$2.7\times10^{-8}$。

关键词:气体绝缘设备;SF_6分解产物;H_2S气体检测;光声光谱;多通光声池
中图分类号:O433.5 **文献标识码**:A **doi**:10.3788/gzxb20235203.0352121

0 引言

H_2S是一种强吸附性、强腐蚀性且具有剧毒的气体,伴随着一股臭鸡蛋气味,人体吸入后则会黏附在肺部,最高允许的体积分数为7.06×10^{-6}。此外,在气体绝缘设备应用方面,该气体会导致设备严重损坏[1]。SF_6因具有优良的绝缘和灭弧性能常在气体绝缘设备中被用作绝缘介质,然而设备内部由于老化或者过热会产生局部放电,导致SF_6分解形成低氟化物,这些低氟化物会再次与设备内部的水和氧气等生成特征气体H_2S[2]。根据我国SF_6气体标准与IEC相关标准的应用规定[3],必须严格执行SF_6气体运行中的质量控制指标,因此对微量H_2S气体的高灵敏度在线监测尤为重要[4]。

目前对于SF_6分解产物主要有非光学检测法和光学检测法。非光学检测法包括气相色谱法和电化学检测法等。气相色谱法[5-7]可以同一时间检测多种气体分解产物,但检测时间较长,且需要载气,不适用于在现场进行连续在线监测。电化学法[8-11]操作简便,但电化学传感器寿命较短,交叉干扰大。非光学检测方法普遍存在灵敏度不够高、交叉干扰大、寿命短以及响应时间长等缺点。光学检测方法是近年来比较常用的新型检测方法,以吸收光谱技术为主,主要包括直接吸收光谱技术和间接吸收光谱技术[12-13],其检测原理都是基于朗伯-比尔定律[14]。光声光谱(Photoacoustic Spectroscopy, PAS)检测技术[15]是一种间接吸收光谱技术,因其具有无需载气、免维护、响应时间快和灵敏度高等优点,相比于非光学检测方法而言,获得了更广泛的关注[16-21]。2015年,山西大学董磊课题组研制了一套基于近红外激光的H_2S微量气体检测系统,采用中心波长为1 582 nm的分布反馈式(Distributed Feedback, DFB)激光器作为光源,利用石英增强型光声光谱传感器作为光声探测装置,对空气背景下的H_2S气体检测极限达到1.42×

基金项目:国家电网有限公司总部科技项目(No. B31205210011),国家自然科学基金(Nos. 62275040, 61905034)
第一作者:马凤翔, njumfx@foxmail.com
通讯作者:陈珂,chenke@dlut.edu.cn
收稿日期:2022-08-01;**录用日期**:2022-11-16

10^{-7}[22]。2016年，武汉大学张晓星等研发了一种悬臂梁增强型光声光谱微量气体检测系统，对SF_6背景气体下的微量H_2S的检测灵敏度达到1.75×10^{-6}[23]，光纤传感技术的快速发展，为ppb量级的H_2S气体检测提供了可能性。2017年，董磊等采用高Q值差分光声池与光纤二极管激光器，对SF_6背景下H_2S的最低检测极限达到1.09×10^{-7}[24]；随后，又采用两个近红外二极管激光器和一个紫外固态激光器，研制了一套ppb量级的多组分气体传感系统，对SF_6背景下H_2S气体的检测极限为8.9×10^{-8}[25]，并实现了SF_6背景下CO、H_2S、SO_2的同时测量。2018年，本研究团队使用中心波长为1 576.3 nm的DFB激光器，并结合自行研制的高信噪比锁相放大器，使SF_6背景下的H_2S气体的检测精度提升至1.5×10^{-8}[26]；随后，又提出了一种基于全光光声光谱技术的高灵敏度微量H_2S气体检测方案，高功率光纤放大器级联DFB激光器作为声学激发光源，光纤悬臂梁麦克风作为光声探测器，在1 576.29 nm的波长下实现了3.3×10^{-8}的检测极限[27]。

本文设计了一种基于共振式多通光声池的SF_6分解产物H_2S检测系统，通过优化多通光声池的参数以及激发光的入射角，使激发光束在光声池缓冲腔两侧的凹面镜上进行多次反射，通过增加光程大幅度提高光声信号的激发效率。采用声学共振放大技术和波长调制-二次谐波检测技术，结合高功率光纤放大器，实现对SF_6背景下微量H_2S气体的高灵敏度检测。

1 基本原理

1.1 共振式光声光谱原理

PAS是一种间接吸收光谱技术，通过将目标气体吸收的光能转换为声波信号，再利用声波传感器对光声信号进行检测，进而测定目标气体的浓度，是一种几乎无背景的吸收光谱技术[28]。与非共振式光声池相比，共振式光声池采用谐振管对光声信号进行放大，可以有效增强光声信号，进而提高气体的检测灵敏度。对于共振式光声池，光声管内声波的波节和波腹按照规律来变化，当激光器的调制频率与光声池共振管的共振频率相同时，光声池处于共振状态[29-30]，此时检测到的光声信号的电压可表示为

$$V=\alpha P_0 R_0 C F \tag{1}$$

式中，α为气体在中心波长下的吸收系数，P_0为激发光源的输出功率，R_0为传感器的灵敏度，C为目标气体的浓度。F为池常数，代表系统将气体吸收的光能转化为声能的能力，增大池常数可有效增强光声信号，表示为

$$F=\frac{2(\gamma-1)Q_j {L_{\mathrm{eff}}}^2}{\pi^2 V_c v} \tag{2}$$

式中，γ为目标气体的热容比，v为气体在谐振腔内的声速，V_c为光声池的体积，Q_j为光声池的质量因数，L_{eff}为有效修正长度。

由于SF_6具有密度大、扩散系数高且比热容低等特殊的物理性质，易受到现场工作设备内部的高气压环境的影响。密度较大的SF_6会影响气体在光声腔内的声速[31]，声速v可表示为

$$v=\sqrt{r_0\frac{P_a}{\rho}} \tag{3}$$

式中，r_0为位移P_a为压强，ρ为SF_6气体的密度。气体的密度与气体在光声池内的声速成反比。光声池的共振频率f与声速相关，可表示为

$$f=\frac{\omega}{2\pi}=\frac{v}{2L} \tag{4}$$

光声池的共振频率与声速成正比，因此光声池的共振频率随着声速减小而降低，采用COMSOL仿真软件对SF_6背景以及N_2背景下的光声池的共振频率进行仿真对比，如图1。在269 K和101.325 kPa的条件下，SF_6背景模拟的归一化的共振频率响应为638 Hz，较N_2背景下的共振频率1 602 Hz降低964 Hz。

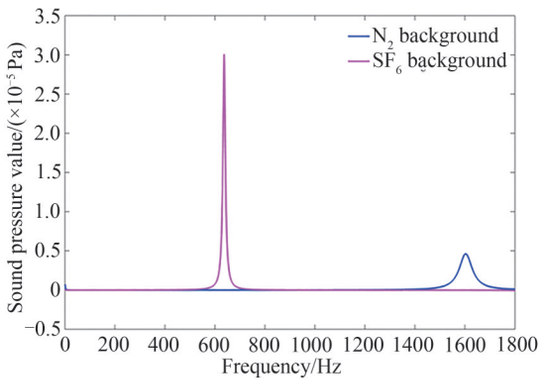

图 1　SF_6及N_2背景下光声池的频率响应

Fig. 1　Frequency response of photoacoustic cell in SF_6 and N_2 background

1.2　多通池原理

PAS技术基于朗伯-比尔吸收定律，通过测定气体在特定波长处或一定波长范围内的吸光度或发光强度，对气体浓度进行测量。当待测气体的浓度不变时，可以通过增加吸收程的长度，增强光声信号的激发光效率[32]。朗伯-比尔定律表示为

$$I(v)=I_0(v)\mathrm{e}^{-C\alpha(v)l} \tag{5}$$

式中，$I(v)$为透射光强，$I_0(v)$为入射光强，C为待测气体的浓度，$\alpha(v)$为气体的吸收系数，L为吸收程的长度，当$C\alpha(v)l\ll 1$时，式(5)可化简为

$$I(v)=I_0(v)\left[1-C\alpha(v)l\right] \tag{6}$$

由准直器准直射入多通池内的激发光，在光声池缓冲腔两侧安装的凹面镜之间来回反射，增强入射光的利用率，进而增强光声信号的激发光功率。图2为模拟的激发光在多通池内进行多次反射的光路图，其理论分析基于ABCD矩阵变换。多通池由两个参数完全相同的镀金凹面镜组成，两个凹面镜之间的距离为L，凹面镜曲率半径为R，直径为d。来自凹面镜N_1方向的入射光沿N_2方向在多通池内传播，到达N_2表面被反射的光，经过光声管返回到N_1表面，以此完成一次反射[33-34]。完成N次反射的矩阵$\boldsymbol{M}$表达式为

$$M=\begin{bmatrix} 1-\dfrac{2L}{R} & 2L\left(1-\dfrac{L}{R}\right) \\ -4R\left(1-\dfrac{L}{R}\right) & -6\dfrac{L}{R}+4\dfrac{L^2}{R^2}+1 \end{bmatrix}^N \tag{7}$$

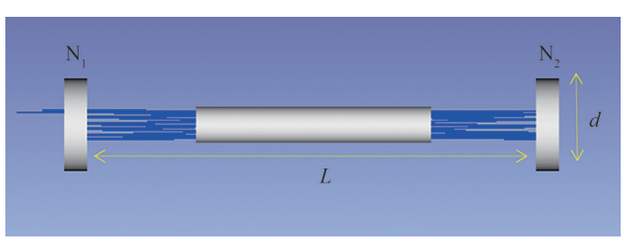

图 2　模拟反射光路图

Fig. 2　Diagram of the simulated reflected light path

为保证激发光反射的光斑始终照射在两凹面镜上，矩阵$\boldsymbol{M}$应保持有限，凹面镜上的光斑分布为椭圆形，表达式(X_n, Y_n)满足以下关系

$$X_n=A\sin(n\theta+\alpha) \tag{8}$$

$$Y_n=B\sin(n\theta+\beta) \tag{9}$$

式中，θ为凹面镜上两相邻两光斑之间的角度，入射凹面镜上光斑的点数为N，反射的总次数为$2N$，总光程为$2NL$。

2 光声气体检测系统设计

2.1 多通光声池的设计

多通光声池由共振管以及两个缓冲腔构成，共振管的长度与内径分别为100 mm和8 mm。在一定程度内增大共振管的内径会进一步增加光线反射次数，增加光的吸收路径长度。然而，共振管的体积随着内径的增大而大幅提高，增加气体交换时间的同时降低了气体检测灵敏度。为增加激发光的光程，在缓冲腔的两侧同轴对称安装两个参数相同的镀金凹面镜，凹面镜的尺寸为25 mm，曲率半径为500 mm，反射率达到98%，为激发光的多次反射提供了可能。反射光点的数量与入射光的角度密切相关，通过精密的光学设计和仿真优化了激发光的入射角度。共振管的内径为8 mm，不恰当的入射光角度会使光线在池壁上发生反射，导致反射次数减少，并且增大光声管壁吸收产生的本底噪声。图3(a)为凹面镜上的光斑分布，当光斑数量最多且不重叠均匀分布时的入射角为0.6°，模拟出的激发光源在多通池内的反射次数达到20次。图3(b)是采用红色指示激光调试的多通池内的多次反射光斑，该测试结果与光路仿真基本一致。

(a) Illustration of simulated light spot　(b) Experimental adjustment of light spot schematic

图3 仿真与实验调节光斑分布示意

Fig. 3 Schematic of simulation and experimental adjustment of spot distribution

2.2 高功率近红外可调谐光声激光光源

SF_6特征分解产物H_2S在近红外与中红外波段都具有谱线吸收峰，虽然中红外吸收波段具有较强的吸收峰，但中红外波段的激光器较昂贵，因此选择近红外波段。图4(a)和4(b)是H_2S气体在近红外处的吸收谱线与模拟的波长调制下气体吸收光所产生的二次谐波，CO_2在近红外波段也具有吸收峰，且气体绝缘设备中存在一定浓度的CO_2气体，会对设备中H_2S气体的检测产生干扰。在1 574.56 nm吸收波段处，H_2S气体吸收系数较高且CO_2对其的干扰较小，因此选择1 574.56 nm作为激发光源的中心波长，采用近红外DFB激光器级联高功率掺铒光纤放大器(Erbium Doped Fiber Amplifier, EDFA)作为系统的激发光源，EDFA输出功率为500 mW，实现光信号的有效放大。

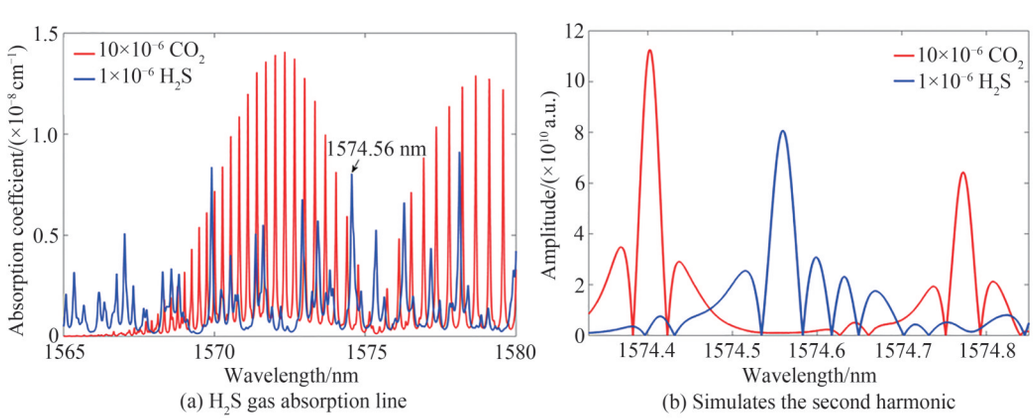

(a) H_2S gas absorption line　(b) Simulates the second harmonic

图4 H_2S吸收谱线的选择

Fig. 4 Selection of H_2S absorption lines

2.3 激光光声光谱气体检测系统设计

光声光谱微量气体检测系统示意如图5，DFB激光器的输出光在连接工作功率为500 mW的EDFA后，采用单模光纤与准直器将光源准直进入光声池。DFB激光器的中心波长为1 574.56 nm，激光驱动电路控制温度和电流。DFB激光器的波长被工作频率为0.1 Hz的低频锯齿波和高频正弦波组成的电流信号驱动，随着驱动电流的增加而变长，实现波长扫描。光声池采用黄铜材质，由一个共振管和两个缓冲室构成，光声池两侧装有凹面反射镜，实现激发光在光声池内的多次反射。电容式传感器探测激发产生的光声信号，用于麦克风探测的小孔的直径和长度分别为2 mm和1 mm。由传感器探测到的信号被基于现场可编程门阵列（Field Programmable Gate Array，FPGA）的锁相放大器处理，再由LabVIEW程序获取到由波长调制技术检测到的二次谐波信号，最终反演出目标气体的浓度。

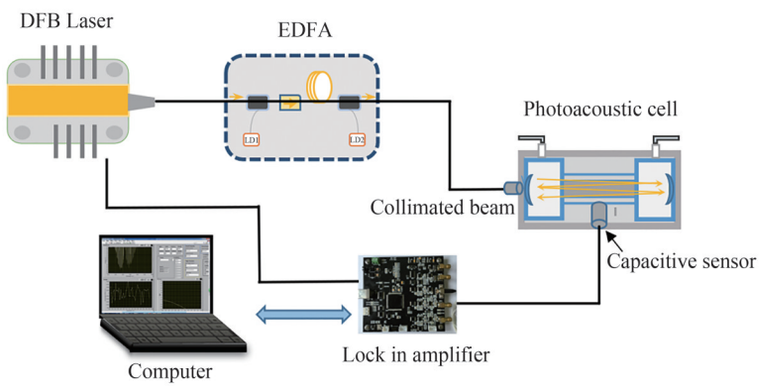

图5 光声光谱微量气体检测系统示意

Fig.5 Schematic of the photoacoustic spectroscopy trace gas detection system

3 实验结果分析与讨论

3.1 调制参数的优化

通过对调制参数幅值的优化，可有效提升基于波长调制-二次谐波检测技术光纤放大激光光声光谱微量气体检测系统的光声信号幅值。将体积分数为100×10^{-6}的H_2S/N_2与50×10^{-6}的H_2S/SF_6的混合气体先后通入到多通池内。实验中，对激光器进行恒温控制，通过光谱仪将其中心波长调制到1 574.56 nm。设置激光器的调制电流使其从0.5 mA开始增加，分别得到N_2背景以及SF_6背景下不同调制电流的H_2S气体的光声信号，如图6。当DFB激光器调制电流设置为3.5 mA时，系统检测的H_2S气体的光声信号幅值最高，N_2背景下H_2S气体的光声信号幅值为648 μV；SF_6背景下H_2S的光声信号幅值为484 μV。

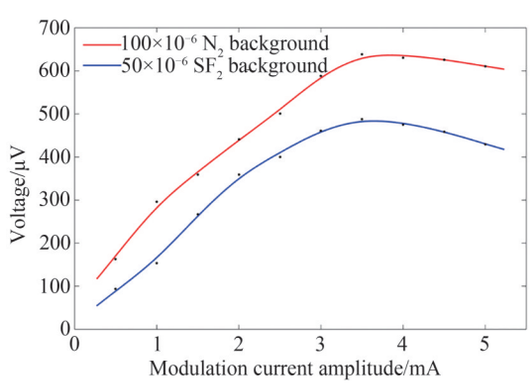

图6 光声信号幅值与调制电流的关系

Fig. 6 The relationship between photoacoustic signal amplitude and modulation current

3.2 多通光声池的频率响应

通过调节激光器的调制频率，可获得多通光声池的共振频率。实验中，向多通光声池内通入体积分数

为100×10^{-6}的H_2S/N_2与50×10^{-6}的H_2S/SF_6的标准气体，控制激光器的输出波长为1 574.56 nm，将激光器的调制频率从100 Hz扫描到1 000 Hz。背景气体的不同导致光声池的共振频率有较大的差异，图7是N_2背景以及SF_6背景下光声池频率响应的对比，通过MATLAB样条插值，采集到光声池共振频率所对应的光声信号的峰值。当二次谐波的调制频率为319 Hz时，即光声池的共振频率为638 Hz，检测到的SF_6背景下H_2S气体的光声信号幅值最高，光声信号为484 μV；当二次谐波的调制频率为801 Hz时，光声池的共振频率为1 602 Hz，检测到的N_2背景下H_2S气体的光声信号幅值最强，光声信号为648 μV，实验结果与仿真结果一致。对于共振式光声池来说，只有当光声信号频率与光声池的共振频率相匹配时，所探测到的光声信号幅值最大，在检测SF_6背景下H_2S时将DFB激光器的正弦调制频率设置为319 Hz。

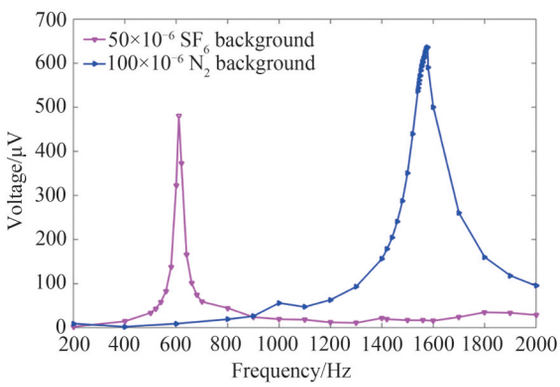

图7 不同背景气体下多通池的共振频率

Fig. 7 Resonance frequencies of multi-pass cell under different background gases

3.3 浓度响应测试与检测极限分析

为了检测多通光声池对待测气体浓度的响应程度并验证仿真分析的正确性，采用两侧不加凹面镜的单次反射光声池进行比较，通入体积分数为50×10^{-6}的H_2S/SF_6的气体。如图8，单程吸收的光声信号幅值为39 μV，多程吸收的光声池信号为484 μV，是单次反射光声池的16倍。

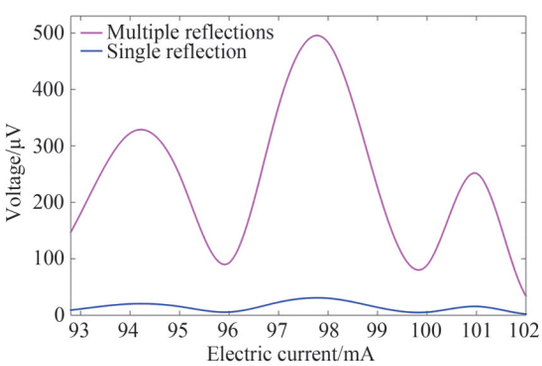

图8 单次反射与多次反射光声信号幅值

Fig. 8 Single and multiple reflection photoacoustic signal amplitudes

将高纯SF_6气体与体积分数为50×10^{-6}的H_2S/SF_6混合气体以一定的比例进行混合，配置出不同体积分数的H_2S/SF_6混合气体，气体体积分数分别为50×10^{-6}、37.5×10^{-6}、25×10^{-6}和12.5×10^{-6}。将DFB激光器调制电流从92 mA扫描至102 mA，绘制出该调制电流范围内不同体积分数水平H_2S气体的二次谐波信号，如图9(a)。为了分析系统对不同体积分数H_2S的线性响应情况，提取图9(a)中不同体积分数的信号峰值进行线性拟合，可获得光声信号与体积分数之间的关系，如图9(b)。系统对微量H_2S气体检测的响应度为9.59×10^{-6} μV，计算得出R^2为0.999，可见系统对于浓度不高于50×10^{-6}的H_2S气体展现良好的线性响应。

为了评估系统的最小检测极限（Minimum Detection Limit，MDL），将高纯SF_6气体持续通入多通池内，用来测量系统的噪声水平。实验过程中激光器的中心波长为1 574.56 nm，锁相积分时间为10 s，记录噪声值，

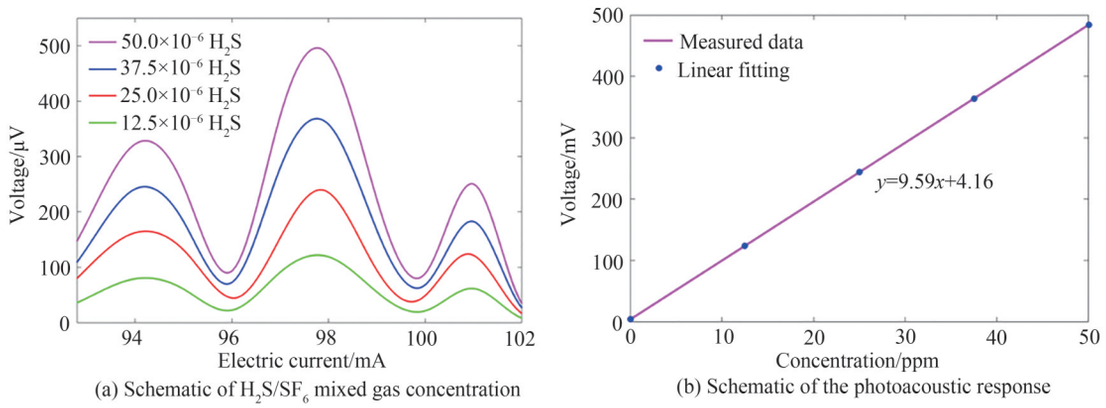

图 9　光声响应与H_2S/SF_6混合气体体积分数的关系

Fig. 9　Relationship between photoacoustic response and H_2S/SF_6 mixed gas concentration

如图 10(a)，噪声的标准差(1σ)为 0.85 μV。根据HITRAN数据库，在常温常压下，H_2S气体在 1 574.56 nm处的吸收系数为 7.96×10^{-3} cm^{-1}。系统对微量H_2S气体的检测灵敏度为 9.59×10^{-6} μV，基于以上数值，NNEA系数计算为 2.23×10^{-9} $cm^{-1}\cdot W\cdot Hz^{-1/2}$。对 1 000 s时间内的噪声进行阿兰方差分析，如图 10(b)，阿兰方差分析结果表明，当平均时间为 100 s时，系统检测极限为 2.7×10^{-8}。

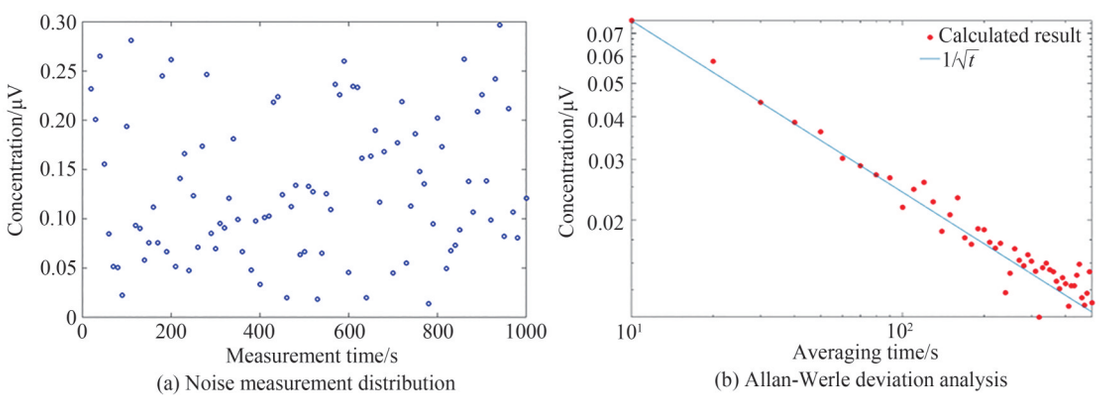

图 10　Allan-Werle方差分析结果

Fig. 10　Allan-Werle deviation analysis results

4　结论

本文设计了一种基于多程吸收激光光声光谱的SF_6分解产物H_2S气体检测系统，采用近红外可调谐DFB激光器级联高功率EDFA作为系统的激发光源。激光器中心波长为 1 574.56 nm，EDFA输出功率为 500 mW，采用共振式多通光声池，光声信号较单次反射光声池放大 16 倍。由于SF_6气体不同于空气的物理性质，光声池共振频率降至 638 Hz。系统测试结果表明，该系统对SF_6背景中H_2S气体的检测响应为 9.59×10^{-6} μV。通过阿伦方差分析，平均时间为 100 s时，系统检测极限为 2.7×10^{-8}。设计的基于多程吸收激光光声光谱的SF_6分解产物H_2S气体检测系统具有高精度、良好的线性度以及稳定的测量能力，在SF_6气体绝缘设备的应用中具有较好的前景。

参考文献

[1] TANG Ju, YANG Xu, YANG Dong, et al. Using SF_6 decomposed component analysis for the diagnosis of partial discharge severity initiated by free metal particle defect[J]. Energies, 2017, 10(8): 1119.

[2] CUI Ruyue, DONG Lei, WU Hongpeng, et al. Highly sensitive and selective CO sensor using a 233 μm diode laser and wavelength modulation spectroscopy[J]. Optics Express, 2018, 26(19): 24318.

[3] PENG Wei. Comparison of the application of my country's SF_6 gas standard and IEC related standards [J]. Electric Power Equipment, 2008,(8): 61-63.
彭伟. 我国SF_6气体标准与IEC相关标准的应用比较[J]. 电力设备, 2008,(8): 61-63.

[4] MA Fengxiang, TIAN Yu, CHEN Ke, et al. Detection technology of H_2S and CO_2 based on fiber amplifier enhanced photoacoustic spectroscopy[J]. Acta Optics Sinica, 2021,41(7): 0730002.
马凤翔,田宇,陈珂,等. 基于光纤放大增强型光声光谱的H_2S与CO_2检测技术[J]. 光学学报,2021,41(7): 0730002.
[5] ZHANG Xiaoxing, ZHANG Yin, TANG Ju, et al. Optical technology for detecting the decomposition products of SF_6: a review[J]. Optical Engineering, 2018, 57(11): 110901.
[6] LIU Changlei. Application of gas chromatography in gas safety analysis of petrochemical enterprises [J]. Qilu Petrochemical, 2016, 44(3): 243-245.
刘长雷. 气相色谱法在石化企业气体安全分析中的应用[J]. 齐鲁石油化工, 2016,44(3): 243-245.
[7] OLTHOFF J, VANBRYNT J, HERRON T, et al. Detection of trace disulfur decafluoride in sulfur hexafluoride by gas chromatography/mass spectrometry[J]. Analytical Chemistry, 1991, 63(7): 726-732.
[8] CHEN Changlun, HE Jianbo, LIU Wei, et al. Research progress of electrochemical gas sensors[J]. Sensor World, 2004, (4): 11-15.
陈长伦,何建波,刘伟,等. 电化学式气体传感器的研究进展[J]. 传感器世界, 2004,(4): 11-15.
[9] DONG Ming, ZHANG Chongxing, REN Ming, et al. Electrochemical and infrared absorption spectroscopy detection of SF_6 decomposition products[J]. Sensors, 2017, 17(11): 2627.
[10] YIN Xukun, DONG Lei, WU Hongping, et al. Sub-ppb nitrogen dioxide detection with a large linear dynamic range by use of a differential photoacoustic cell and a 3.5W blue multimode diode laser[J]. Sensors and Actuators B: Chemical, 2017, 247: 329-335.
[11] ZHENG Huadan, LOU Minhan, DONG Lei, et al. Compact photoacoustic module for methane detection incorporating interband cascade light emitting device[J]. Optics Express, 2017, 25(14): 16761-16770.
[12] CHEN Ke, ZHANG Bo, GUO Min, et al. All-optical photoacoustic multigas analyzer using digital fiber-optic acoustic detector[J]. IEEE Transactions on Instrumentation and Measurement, 2020, 69(10): 8486-8493.
[13] CHEN Ke, ZHANG Bo, LIU Shuai, et al. Parts-per-billion-level detection of hydrogen sulfide based on near-infrared all-optical photoacoustic spectroscopy[J]. Sensors and Actuators B: Chemical, 2019, 283: 1-5.
[14] CUI Zhaolun, ZHANG Xiaoxing, CHENG Zheng, et al. Quantitative analysis of SO_2, H_2S and CS_2 mixed gases based on ultraviolet differential absorption spectrometry [J]. Spectrochimica Acta Part A: Molecular and Biomolecular Spectroscopy, 2019, 215: 187-195.
[15] LUO Jin, FANG Yonghua, ZHAO Yandong, et al. Research on the detection of SF_6 decomposition products based on non-resonant photoacoustic spectroscopy[J]. Analytical Methods, 2015, 7(3): 1200-1207.
[16] MA Fengxiang, TIAN Yu, CHEN Ke, et al. Detection technology of H_2S and CO_2 based on optical fiber amplification enhanced photoacoustic spectroscopy[J]. Acta Optics Sinica, 2017,41(7):0703002.
马凤翔,田宇,陈珂,等. 基于光纤放大增强型光声光谱的H_2S与CO_2检测技术[J]. 光学学报,2017,41(7):0703002.
[17] CHA Shenlong, LIU Kun, TAN Tu, et al. Application of photoacoustic spectroscopy in multi-component gas concentration detection[J]. Acta Photonica Sinica, 2017,46(6):0612002.
查申龙,刘锟,谈图,等. 光声光谱技术在多组分气体浓度探测中的应用[J]. 光子学报,2017,46(6):0612002.
[18] YU Rong, JIANG Yuesong. Photoacoustic spectroscopy system with amplitude spectrum and phase spectrum measurement functions[J]. Acta Optica Sinica, 2014, 34(2): 0230001.
余荣,江月松. 一种可同时实现振幅谱与相位谱测量的光声光谱系统[J]. 光学学报,2014, 34(2): 0230001.
[19] WANG Qiang, XU Ke, YAO Yuchen, et al. Recent advances of power-enhanced photoacoustic spectroscopy for gas sensing[J]. Chinese Journal of Lasers, 2018, 45(9): 0911008.
王强,许可,姚晨雨,等. 功率增强型光声光谱气体传感技术的研究进展[J]. 中国激光,2018, 45(9): 0911008.
[20] YUAN Shuai, WANG Guangzhen, FU Dehui, et al. Cross interference characteristics of photoacoustic spectroscopy multi-gas analyzer[J]. Acta Photonica Sinica, 2021,50(4): 0430002.
袁帅,王广真,付德慧,等. 光声光谱多组分气体分析仪的交叉干扰特性研究[J]. 光子学报,2021,50(4): 0430002.
[21] WANG Shutao, CHE Rensheng, WANG Yutian, et al. Research on optical fiber gas sensor based on photoacoustic spectroscopy[J]. China Journal of Laser, 2004,31(8): 979-982.
王书涛,车仁生,王玉田,等. 基于光声光谱法的光纤气体传感器研究[J]. 中国激光,2004,31(8): 979-982.
[22] WU Hongping, DONG Lei, ZHENG Huadan, et al. Enhanced near-infrared QEPAS sensor for sub-ppm level H_2S detection by means of a fiber amplified 1 582 nm DFB laser[J]. Sensors and Actuators B: Chemical, 2015, 221: 666-672.
[23] ZHANG Xiaoxing, CHENG Zheng, LI Xin. Cantilever enhanced photoacoustic spectrometry: quantitative analysis of the trace H_2S produced by SF_6 decomposition[J]. Infrared Physics & Technology, 2016, 78: 31-39.
[24] YIN Xukun, DONG Lei, WU Hongfu, et al. Ppb-level H_2S detection for SF_6 decomposition based on a fiber-amplified telecommunication diode laser and a background-gas-induced high- Q photoacoustic cell[J]. Applied Physics Letters, 2017, 111(3): 031109.
[25] YIN Xukun, DONG Lei, WU Hongping, et al. Highly sensitive photoacoustic multicomponent gas sensor for SF_6

decomposition online monitoring[J]. Optics Express, 2019, 27(4): A224.
[26] CHEN Ke, YUAN Shuai, GONG Zhenfeng, et al. High sensitive detection for SF_6 decomposition component of H_2S based on laser photoacoustic spectroscopy[J]. Chinese Journal of Lasers, 2018, 45(9): 0911012.
陈珂,袁帅,宫振峰,等. 基于激光光声光谱超高灵敏度检测SF_6分解组分H_2S[J].中国激光, 2018, 45(9): 0911012.
[27] CHEN Ke, ZHANG Bo, LIU Shuai, et al. Parts-per-billion-level detection of hydrogen sulfide based on near-infrared all-optical photoacoustic[J]. Sensors and Actuators B: Chemical.2019, 283: 1-5.
[28] ZHAO Nan, LIU Yang, ZHAO Ningyang, et al. Establishment and optimization of photoacoustic cell model in photoacoustic spectrum detection system[J]. Acta Photonica Sinica, 2021,50(7): 0730001.
赵南,刘阳,赵宁阳,等. 光声光谱检测系统中光声池模型的建立与优化[J].光子学报,2021,50(7): 0730001.
[29] CHEN Ke, YANG Beilei, GUO Min, et al. Fiber-optic photoacoustic gas sensor with temperature self-compensation[J]. Optics Letters, 2020, 45(8): 2458-2461.
[30] CHEN Ke, YU Zhihao, GONG Zhenfeng, et al. Lock-in white-light-interferometry-based all-optical photoacoustic spectrometer[J]. Optics Letters, 2018, 43(20): 5038-5041.
[31] CHEN Ke, GUO Min, YANG Beilei, et al. Highly sensitive optical fiber photoacoustic sensor for in situ detection of dissolved gas in oil[J]. IEEE Transactions on Instrumentation & Measurement, 2021,70: 1-8.
[32] ZHAO Xinyu, CHEN Ke, CUI Dongyu, et al. Ultra-high sensitive photoacoustic gas detector based on differential multi-pass cell[J]. Sensors and Actuators B: Chemical, 2022, 368: 132124.
[33] HERRIOTT D, KOGELNIK H, KOMPFNER R. Off-axis paths in spherical mirror interferometers[J]. Applied Optics, 1964, 3(4): 523-526.
[34] ZHANG Zhenxi, ZHOU Hongguang, CHEN Xufei, et al. Design method of variable optical path length multi-pass cell [J]. Applied Physics B, 2021, 127(2): 12.

High-sensitivity Detection Technology of SF_6 Decomposition Product H_2S Based on Multi-pass Photoacoustic Cell

MA Fengxiang[1], ZHAO Yue[1], WANG Nan[2], ZHAO Xinyu[2], GUO Min[2], LI Chenxi[2], ZHU Taiyun[1], HANG Chen[1], CHEN Ke[2]
(1 *Electric Power Research Institute, State Grid Anhui Electric Power Co., Ltd., Hefei* 230601, *China*)
(2 *School of Optoelectronic Engineering and Instrumentation Science, Dalian University of Technology, Dalian* 116024, *China*)

Abstract: SF_6 is applied as an insulating medium in gas-insulated equipment due to its excellent insulation and arc extinguishing properties. However, aging or overheating within the equipment can cause partial discharge, resulting in the decomposition of SF_6 to form low-fluoride compounds, which react with water and oxygen inside the equipment to produce the characteristic gas H_2S. As a decomposition product of SF_6, H_2S is one of the characteristic components of fault diagnosis of gas-insulated equipment, and has strong corrosivity and toxicity. The inferior nature of this gas can lead to serious damage inside the equipment. Therefore, high-sensitivity online monitoring of trace H_2S gas is of great significance for the stable operation of gas-insulated equipment. Detection techniques for SF_6 decomposition products envelop non-optical and optical methods. Beer-Lambert-based Photoacoustic Spectroscopy (PAS) sensing technology is an indirect absorption spectroscopy technique that has gained a wider range of attention than non-optical detection methods due to its advantages of no gas load, no maintenance, fast response time, and high sensitivity. When the concentration of the gas to be measured is unchanged, the excitation light efficiency of the photoacoustic signal can be enhanced by increasing the length of the absorption path. The excitation light injected into the multi-pass cell is collimated by the collimator and reflected back and forth between the concave mirrors installed on both sides of the buffer of the photoacoustic cell. H_2S has a good spectral line absorption peak in the near-infrared band. The near-infrared laser is incident on a multi-pass photoacoustic cell after power amplified, and the excitation efficiency of the photoacoustic signal is greatly improved through multiple optical reflections. Combined with acoustic resonance amplification, optical fiber amplification and wavelength modulation-second harmonic detection technology, a set of photoacoustic spectroscopy gas detection system is built to achieve high-sensitivity detection of trace H_2S

gas in SF_6 background. A 1 574.56 nm near-infrared distributed feedback DFB laser cascaded a high-power Erbium-doped Fiber Amplifier (EDFA) is selected as the excitation light source of the system. A single-mode fiber-optic and a collimator are used to collimate the light source into the photoacoustic cell. The photoacoustic cell consists of a resonant tube and two buffer chambers flanked by concave mirrors. The photoacoustic signals are detected in real time by capacitive sensors, and then processed by a Field-programmable Gate Array (FPGA)-based lock-in amplifier. The second harmonic signals are obtained by the LabVIEW program, and the concentration of the target gas to be detected is calculated. SF_6 is a gas with special physical properties such as high density, high diffusion coefficient and low specific heat capacity, which is easily affected by the high-pressure environment inside the field work equipment. COMSOL simulation software is used to simulate the resonance frequency of the photoacoustic cell in SF_6 background and N_2 background, and the experimental results are consistent with the simulation results. In SF_6 background, the photoacoustic cell resonance frequency is reduced to 638 Hz. In order to effectively improve the amplitude of the photoacoustic signal of the fiber amplification laser photoacoustic spectroscopy detection system based on wavelength modulation-second harmonic detection technology, the amplitude of the modulation parameters is optimized. When the modulation current of the DFB laser is set to 3.5 mA, the amplitude of the photoacoustic signal detected by the system is the highest. To assess the response of the multi-pass photoacoustic cell to the measured gas concentration, the high-purity SF_6 gas is mixed with a H_2S/SF_6 mixture of 50 ppm in a certain proportion, and the system shows a good linear response of 9.59 μV/ppm for H_2S gas concentrations up to 50 ppm. A continuous charge of pure SF6 gas into the multi-pass cell is used to measure the noise level and evaluate the Minimum Detection Limit (MDL) of the system. The standard deviation (1σ) of the noise is 0.85 μV. The experimental results show that the Normalized Noise Equivalent Absorption (NNEA) coefficient is 2.23×10^{-9} $cm^{-1}\cdot W\cdot Hz^{-1/2}$. Allan deviation analysis is performed on the noise over a time period of 1 000 s. The Allan deviation result shows that when the averaging time is 100 s, the MDL of the system is 27 ppb. The system gradually stabilized with the increase of the mean time. The detection limit on the order of ppb provide a favorable solution for diagnosing the failure of gas insulation equipment.

Key words: Gas insulation equipment; SF_6 decomposition products; H_2S gas detection; Photoacoustic spectroscopy; Multi-pass photoacoustic cell

OCIS Codes: 280.4788; 300.1030; 300.6340; 300.6360

Foundation item: The Technology Project of State Grid Co., Ltd. Headquarters (No. B31205210011), National Natural Science Foundation of China (Nos. 62275040, 61905034)